

# Steady-state and bistable superradiant phases of an atomic beam traversing an optical cavity

Simon B. Jäger,<sup>1</sup> Haonan Liu,<sup>1</sup> Athreya Shankar,<sup>1</sup> John Cooper,<sup>1</sup> and Murray J. Holland<sup>1</sup>

<sup>1</sup>*JILA and Department of Physics, University of Colorado, Boulder, Colorado 80309-0440, USA.*

We investigate the different emission regimes of a pre-excited and collimated atomic beam passing through an optical cavity. In the regime where the cavity degrees of freedom can be adiabatically eliminated, we find that the atoms undergo superradiant emission if the collective linewidth exceeds transit-time broadening. We analyze the case where the atomic beam is not precisely perpendicular to the cavity axis and find a phase of continuous light emission similar to steady-state superradiance for a sufficiently small tilt of the atomic beam. However, if the atoms travel more than half a wavelength along the cavity axis during one transit time we predict a dynamical phase transition to a new bistable superradiant regime. In this phase the atoms undergo collective spontaneous emission with a frequency that is either blue or red detuned of the free-space atomic resonance. We analyze the different superradiant regimes and the quantum critical crossover boundaries. We examine in particular the spectrum of the emitted light and show that the linewidth exhibits features of a critical scaling close to the phase boundaries.

Atomic ensembles in optical cavities provide a versatile testbed for the engineering and study of many-body effects that are both fundamentally interesting and have practical applications. In these systems, the cavity mode serves as a common and intrinsically lossy channel that enables strong light-atom and atom-atom interactions. Therefore these setups have been used to simulate exotic many-body quantum phases [1–10], to analyze collective dynamics in the presence of dissipation [11–16], and also to develop technologies that use collective effects to enhance metrological applications [17–23].

A remarkable example of such technology is the steady-state superradiant laser [22, 23]. This laser works in a regime where the lifetime of cavity photons is orders of magnitude shorter than the lifetime of the coherent dipoles. In this regime, coherences are stored in the superradiant collective dipole [24, 25] of the atomic gas. Consequently, lasing with ultra-narrow linewidth can be achieved while the light field remains robust with respect to cavity length changes [22, 23, 26–30]. Beside this technological feature, this setup also provides a platform to study out-of-equilibrium dynamics of incoherently driven dipoles where the cavity photons that mediate long-range interactions inherently transport quantum noise. The rich physics of this driven-dissipative system has been connected to time crystals [31–35], synchronization [36–40], and dynamical phase transitions [41–45].

In this Letter, we study the dynamical superradiant phases that manifest when a dense collimated atomic beam passes through an optical cavity. We investigate the case where all the atoms have the same fixed velocity  $\mathbf{v} = (v_x, v_z)$ , where  $v_x$  ( $v_z$ ) is the longitudinal (transverse) component perpendicular (parallel) to the cavity axis (Fig. 1a). Each atom is described as a two-level system representing an optical dipole with transition frequency  $\omega_a$  between its excited state  $|e\rangle$  and ground state  $|g\rangle$ . We assume the atoms are pre-excited in  $|e\rangle$  before they enter the cavity. Once in the cavity, the atoms

interact with a single mode of frequency  $\omega_c$  that is on resonance, i.e.,  $\omega_c = \omega_a$ . Coherence arises in this system solely due to the coherent coupling between the atomic beam and the cavity mode since there are no external lasers driving the atoms while they are inside the cavity volume. The atom-cavity coupling is characterized by a vacuum Rabi frequency  $g$  defined at the maximum of the corresponding cavity mode function  $\eta(\mathbf{x})$  (Fig. 1b).

We investigate the so-called bad cavity or good atom regime for the cavity linewidth  $\kappa$ . In particular, we assume that the cavity decays more rapidly than the atomic transit time  $\tau$ , i.e.,  $\kappa^{-1} \ll \tau$ , and the Rabi splitting due to the coherent atom-cavity exchange is unresolvable, i.e.,  $\sqrt{N}g \ll \kappa$ , where  $N$  is the intracavity atom number. In this regime, the field mode mediates an all-to-all interaction between the atoms and exposes the dipoles to quantum noise. We neglect spontaneous emission and other dephasing mechanisms, that is, we assume that  $\tau$  is much shorter than the free-space population decay time  $T_1$  and the single-atom dephasing time  $T_2$ . Our analysis is based on a semiclassical description of the atomic dipoles and, in addition, we treat the atomic motion as a ballistic phase space trajectory and ignore optomechanical forces.

Within this framework, we examine the dynamics of the densities  $s_a(\mathbf{x}, t) = \sum_j s_j^a \delta(\mathbf{x} - \mathbf{x}_j)$ ,  $a \in \{x, y, z\}$ ,  $s_j^a$  describes the  $c$ -number equivalent of the Pauli matrix  $\hat{\sigma}_j^a$  for the dipole component, and  $\mathbf{x}_j = (x_j, z_j)$  is the position of atom  $j$ . The dynamics of the densities after the adiabatic elimination of the cavity are described by the following Klimontovich-like stochastic equations [46];

$$\frac{\partial s_x}{\partial t} + \mathbf{v} \cdot \nabla_{\mathbf{x}} s_x = \frac{\Gamma_c}{2} \eta(\mathbf{x}) J_x s_z + \mathcal{S}_x, \quad (1)$$

$$\frac{\partial s_y}{\partial t} + \mathbf{v} \cdot \nabla_{\mathbf{x}} s_y = \frac{\Gamma_c}{2} \eta(\mathbf{x}) J_y s_z + \mathcal{S}_y, \quad (2)$$

$$\frac{\partial s_z}{\partial t} + \mathbf{v} \cdot \nabla_{\mathbf{x}} s_z = -\frac{\Gamma_c}{2} \eta(\mathbf{x}) [J_x s_x + J_y s_y] + \mathcal{S}_z. \quad (3)$$

These equations are presented in the reference frame

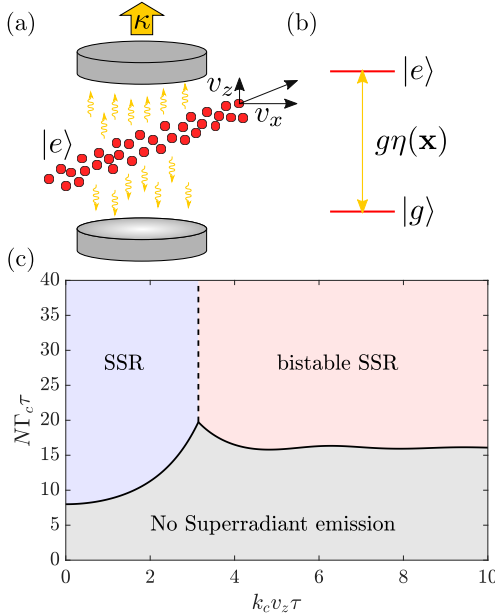


FIG. 1. (a) Atoms are pre-excited and pass through a lossy optical cavity. (b) Two-level atoms resonantly exchange photons with the cavity mode with a spatially dependent coupling  $g\eta(\mathbf{x})$ . (c) The resulting phase diagram describing the light emission for different values of the Doppler shift,  $k_c v_z$ , and the collective linewidth,  $NT_c$ , both in units of the inverse transit time,  $1/\tau$ . For small values of  $NT_c\tau$  we find no superradiant emission. For sufficiently large values of  $NT_c\tau$ , regimes of either steady-state superradiance (SSR) or bistable SSR are observed depending on the magnitude of  $k_c v_z \tau$ .

rotating with frequency  $\omega_a$ . The left-hand sides of Eqs. (1-3) describe the free flight of the atoms where  $\mathbf{x} = (x, z)$  and  $\nabla_{\mathbf{x}} = (\partial_x, \partial_z)$ . The first term on the right-hand side of each equation characterizes the collective decay mediated by the cavity field. Here,  $\Gamma_c = g^2/\kappa$  is the single-atom emission rate into the cavity mode and  $J_a = \int d\mathbf{x} \eta(\mathbf{x}) s_a(\mathbf{x}, t)$  are the collective dipole components with  $a \in \{x, y\}$ . In this Letter we assume the cavity mode function to be  $\eta(\mathbf{x}) = \cos(k_c z) [\Theta(x + w) - \Theta(x - w)]$ , where  $\Theta(x)$  is the Heaviside step function,  $w = v_z \tau/2$  is the cavity beam waist,  $k_c = 2\pi/\lambda$  is the wavenumber, and  $\lambda$  is the optical wavelength. The  $\mathcal{S}_a$  terms are stochastic variables that encapsulate the effective cavity shot noise that arises from the finite output coupling. They are described by  $\mathcal{S}_a(\mathbf{x}, t) = \eta(\mathbf{x}) \mathcal{F}_a s_z$  and  $\mathcal{S}_z(\mathbf{x}, t) = -\eta(\mathbf{x}) [\mathcal{F}_x s_x + \mathcal{F}_y s_y]$ , where  $\mathcal{F}_x$  and  $\mathcal{F}_y$  are independent Wiener processes that satisfy  $\langle \mathcal{F}_a(t) \rangle = 0$  and  $\langle \mathcal{F}_a(t) \mathcal{F}_b(t') \rangle = \Gamma_c \delta_{ab} \delta(t - t')$ , where  $a, b \in \{x, y\}$ . The prescribed condition that new atoms are introduced in state  $|e\rangle$  leads to a boundary condition  $s_z(x = -w, z, t) = N/(2w\lambda)$ . This is derived assuming  $\lambda$ -periodic boundary conditions in  $z$  direction. In order to describe the quantum fluctuations of the introduced dipoles it is necessary to establish the correct magnitudes of the second moments [47]. To do this, we initial-

ize the  $s_x$  and  $s_y$  components with the aid of a simulated noise process that is defined by the following properties;  $s_a(x = -w, z, t) = W_a(z, t)$ , with  $\langle W_a(z, t) \rangle = 0$  and  $\langle W_a(z, t) W_b(z', t') \rangle = N/(2w\lambda) \delta_{ab} \delta(z - z') \delta(t - t')/v_x$ .

We first solve Eqs. (1-3) within the scope of a mean-field approximation, where we assume  $s_a \approx \langle s_a \rangle$ ,  $a \in \{x, y, z\}$ , and calculate the expectation values of the individual dipole components. Here the expectation value  $\langle \cdot \rangle$  denotes an average over different initializations and different noises. We observe that there is a non-superradiant solution with  $\langle J_a \rangle = 0 = \langle s_a(\mathbf{x}, t) \rangle$ ,  $a \in \{x, y\}$ , and  $\langle s_z(\mathbf{x}, t) \rangle = N/(2w\lambda)$ . In this case the atoms essentially do not interact with the cavity and there is no emission of photons. However, this mean-field solution is in general not stable with respect to the physical noise sources that are intrinsically present. Fluctuations of the dipoles and cavity shot noise can initiate an emission process that leads to a collective emission into the cavity. In order to find the threshold for this effect we calculate the stability of the non-superradiant solution with respect to a small fluctuation  $\delta s_a$  around  $s_a = 0$ . This fluctuation induces a small perturbation in the collective dipole  $\delta J_a = \int d\mathbf{x} \eta(\mathbf{x}) \delta s_a$ . We describe the solution in the supplemental material (SM) [48], where we calculate the exponent  $\nu_0$  that governs the decay or amplification of the fluctuations in the dipoles,  $\delta J_a \propto e^{\nu_0 t}$ . If  $\text{Re}(\nu_0)$  is negative we anticipate the fluctuations to be damped. Otherwise, if  $\text{Re}(\nu_0)$  is positive the fluctuations are exponentially amplified leading to a collective emission and a dynamical phase transition. The boundary between the regime of no superradiant emission and that of superradiant emission is visible in Fig. 1c as solid black line. Superradiant emission emerges when the transit time broadening  $1/\tau$  is smaller than the collective linewidth  $NT_c$ . In this case the atoms build up a macroscopic collective dipole resulting in  $J_x^2 + J_y^2 \sim N^2$  that signifies the superradiant phases of the atomic beam and leads to a non-vanishing number of cavity photons.

We now focus entirely on the superradiant emission regime. In particular, we are interested in understanding the effect of  $v_z$  along the cavity axis that leads to a transverse Doppler shift in the frequency of emitted photons. For a single atom, the emission of photons into the direction of motion shifts the frequency to the blue while emission in the opposite direction shifts the frequency to the red. Remarkably, we observe that for small velocities  $v_z$  the atomic beam undergoes superradiant emission that is resonant with the bare atomic resonance frequency. In order to demonstrate this behavior, we show in Fig. 2a the spectrum

$$S(\omega) \propto \left| \int_0^T dt e^{i\omega t} \langle J^*(t + t_0) J(t_0) \rangle \right|, \quad (4)$$

where  $t_0 \gg \tau$  is a sufficiently large time after which the system has reached a stationary state and

$J(t) = [J_x(t) - iJ_y(t)]/2$ . The time  $T$  is the integration time after  $t_0$  (see caption of Fig. 2). For  $k_c v_z \tau = 2\pi \times 0.3$ , i.e. when each atom traverses 0.3 wavelengths along the cavity axis during the transit time, the spectrum shows a narrow Lorentzian peak at  $\omega = 0$  corresponding to continuous superradiant emission at the transition frequency of the atomic dipole. We label this phase as SSR, due to the similarities with steady-state superradiance (Fig. 1c).

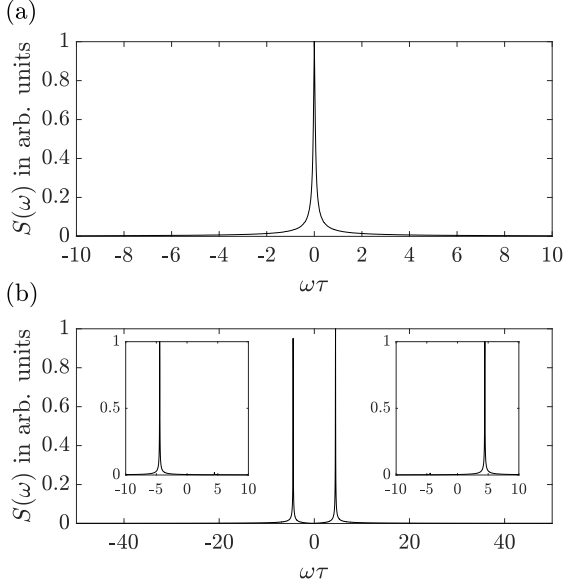


FIG. 2. The spectrum  $S(\omega)$  (Eq. (4)) as a function of the frequency  $\omega$  in units of  $1/\tau$  in the SSR phase for  $k_c v_z \tau = 2\pi \times 0.3$  (a) and in the bistable SSR phase  $k_c v_z \tau = 2\pi \times 0.8$  (b). For the simulation we used  $N\Gamma_c\tau = 30$ ,  $N = 800$ , and a total integration time of  $t_0 + T = t_{\text{sim}} = 2000\tau$ . The spectra are calculated using 500 independent initializations and after a time  $t_0 = 10\tau$  where the system reaches for good approximation the steady state. The two insets in subplot (b) show the averaged spectrum of the trajectories that correspond to a negative frequency  $\omega\tau \approx -4.46$  (238 trajectories) and positive frequency  $\omega\tau \approx 4.46$  (262 trajectories).

While this behavior remains stable at first as  $v_z$  is increased, once a critical velocity is reached we observe a threshold where a qualitatively different behavior is realized. As an example, we show  $S(\omega)$  for  $k_c v_z \tau = 2\pi \times 0.8$  in Fig. 2b, which corresponds to each atom traversing 0.8 wavelengths along the cavity axis. In this case, the spectrum exhibits two narrow Lorentzian peaks that are symmetrically shifted from the resonance frequency of the atoms. While the form of the spectrum suggests simultaneous emission with both frequencies, we find that the atomic beam will randomly undergo superradiant emission with either the red or the blue detuned frequency. The random choice is seeded by the first emission with probability of 0.5 for each of the two possibilities. Subsequently collective spontaneous emission events will amplify the light field with the corresponding frequency.

To further demonstrate this behavior, we illustrate in

the left (right) inset of Fig. 2b the emission spectrum that corresponds to trajectories that emit with red (blue) detuned frequencies. Since we have a finite number of initializations we may observe a slight imbalance of red-detuned frequencies with respect to blue-detuned frequencies in each specific trial. This imbalance can be seen as different heights in the spectrum shown in Fig. 2b. In the insets we see only one peak supporting our claim that superradiant emission appears for the shown parameters only on one sideband. Because of the bistable nature of the superradiant peaks, this is reminiscent of optical bistability of intensity solutions [49], and consequently we refer to this phase as bistable SSR (Fig. 1c). On long timescales we expect mode hopping since there is a finite probability for the system to switch between the sidebands. In our numerics, we have observed that this process is more frequent close to the transition from SSR to bistable SSR as we report in the SM [48].

We will now investigate properties of the collective dipole across the SSR to bistable SSR transition that indicate a critical behavior at the threshold. The results are calculated for  $N\Gamma_c\tau = 20$ , close to the non-superradiant regime, and for  $N\Gamma_c\tau = 30$ , well inside of the superradiant regime. In Fig. 3a-d, we show  $\langle J^*J \rangle/N^2$  (a-b) and the emission frequency  $\omega$  (c-d) as a function of  $k_c v_z \tau$ . The solid lines are mean-field results and the circles, stars are the results of  $c$ -number simulations according to Eqs. (1-3). Mean field theory predicts a non-analytical behavior of both,  $\langle J^*J \rangle/N^2$  and  $\omega$ , at the theoretically predicted threshold  $k_c v_z \tau = \pi$  (vertical gray dashed line, see SM [48]). It shows a kink-like local minimum for  $\langle J^*J \rangle/N^2$  and a bifurcation of  $\omega$  at the threshold that is in agreement with the simulations. In general we find that the non-analyticities are smoothed by noise and finite size effects. The rather large discrepancies between the mean-field results and the simulations in Fig. 3a are likely due to these effects that are more pronounced close to a tri-critical point where SSR, bistable SSR, and the non-superradiant emission phases meet (the tri-critical point is at  $N\Gamma_c\tau = 2\pi^2$  and  $k_c v_z \tau = \pi$ ).

Critical features of the SSR to bistable SSR transition are highlighted in the linewidth  $\Gamma$  of the output field in Fig. 3e-f obtained by integrating Eqs. (1-3). We observe that  $\Gamma$  becomes maximal close to the theoretically predicted threshold  $k_c v_z \tau = \pi$ . The mean-field solution cannot predict the linewidth since in the absence of noise the phase of the collective dipole is stable on arbitrary timescales. However, the addition of input noise  $W_a(z, t)$  and cavity noise  $\mathcal{S}_a(\mathbf{x}, t)$ ,  $a \in \{x, y\}$ , leads to phase diffusion of the collective dipole. The resulting values of  $\Gamma$  can be calculated in the SSR phase and are plotted as the solid lines in Fig. 3e-f (see SM [48]). These curves are in very good agreement with the  $c$ -number simulations (circles, stars) well inside of the SSR phase but predict a diverging linewidth at the critical point. We expect that this divergence should be recovered by the  $c$ -number sim-

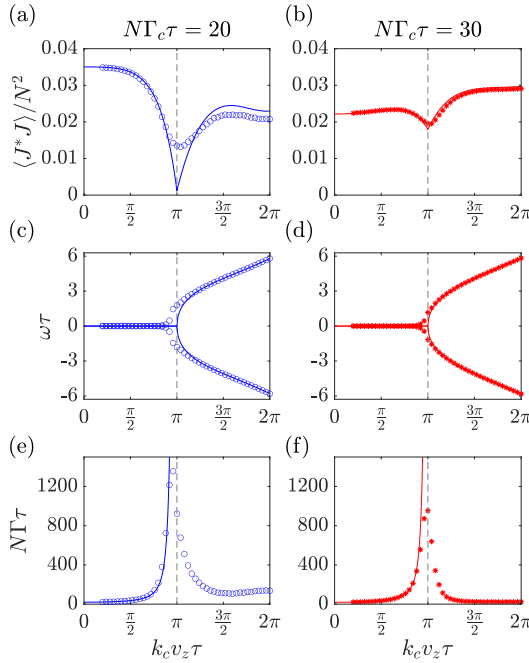


FIG. 3. The collective dipole  $\langle J^* J \rangle / N^2$  (a)-(b), the frequency of the light  $\omega$  in units of  $1/\tau$  (c)-(d), and the linewidth  $\Gamma$  in units  $1/(N\tau)$  (e)-(f) as functions of  $k_c v_z \tau$ . Subplot (a), (c), (e), and (b), (d), (f) are calculated for  $NT_c \tau = 20$  and  $NT_c \tau = 30$ , respectively. The circles and stars correspond to numerical simulations, the solid lines represent analytical solutions in the limit  $N \rightarrow \infty$ . The vertical gray dashed lines show the transition from SSR to bistable SSR. The values of  $\omega$  in (c)-(d) and  $\Gamma$  in (e)-(f) have been calculated by fitting  $\langle \text{Re}[J^*(t+t_0)J(t_0)] \rangle / \langle |J(t_0)|^2 \rangle$  with  $\cos(\omega t + \phi_0) e^{-\Gamma t/2}$  and  $t_0 = 10\tau$ . The simulations are performed with  $N = 800$  and an integration time of  $t_{\text{sim}} = 100\tau$ .

ulations in the limit  $N \rightarrow \infty$ .

In order to support this claim, we plot  $\Gamma$  in units of  $1/\tau$  for different values of  $N$  in a log-log plot to illustrate the scaling of the linewidth with the number of atoms,  $\Gamma \tau \propto N^\alpha$  (Fig. 4). We show the scaling well inside the SSR phase for  $k_c v_z \tau = \pi/2$  (green crosses), well inside the bistable SSR phase for  $k_c v_z \tau = 3\pi/2$  (red stars), and at the theoretically predicted threshold  $k_c v_z \tau = \pi$  (blue circles). The values of the exponent  $\alpha$  governing the scaling relation  $\Gamma \tau \propto N^\alpha$  in the three regimes are extracted using a linear fit and are reported in the caption of Fig. 4. For the parameters well inside of the SSR or bistable SSR phases we obtain an exponent that is  $\alpha \approx -1$ . This implies that for given values of  $k_c v_z \tau$  and  $NT_c \tau$ ,  $\Gamma$  is a constant when calculated in units of  $1/(N\tau) \propto \Gamma_c$ . This claim is also supported by our theoretical description well inside the SSR phase (see SM [48]).

At the critical point  $k_c v_z \tau = \pi$ , mean-field theory still predicts a zero linewidth, and yet the phase diffusion argument anticipates a diverging linewidth. Our numerical simulations here show that there exists a critical scaling with an exponent  $\alpha \approx -0.3$ . In units of  $1/(N\tau)$

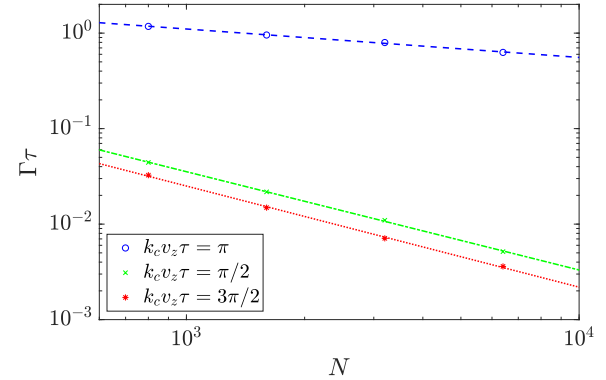


FIG. 4. The linewidth  $\Gamma$  in units of  $1/\tau$  as a function of the intracavity atom number  $N$  for  $NT_c \tau = 30$  in a log-log plot. The blue circles, green crosses, and red stars correspond to different values of  $k_c v_z \tau$  (see legend) at the threshold, in the SSR phase, and in the bistable SSR phase. The blue dashed, green dashed-dotted, and red dotted lines are linear fits according to  $\Gamma \tau \propto N^\alpha$  with  $\alpha = -0.30$ ,  $\alpha = -1.03$ , and  $\alpha = -1.06$ , respectively. For every  $N$  we average over  $4.8 \times 10^5 / N$  trajectories with a simulation time  $t_{\text{sim}} = 100\tau$ . Every point is calculated using the fit as described in the caption of Fig. 3.

the linewidth scales as  $N^{1+\alpha} \approx N^{0.7} \rightarrow \infty$ , supporting our theoretical prediction visible in Fig. 3f of a diverging linewidth using the phase diffusion model. This divergence is reminiscent of the quantum critical region [50] that occurs at finite temperature in an equilibrium quantum phase transition where scaling laws provide the potential for extreme sensitivity to model parameters.

A bifurcation in the emission spectrum and a critical scaling of the linewidth has also been reported for a synchronization transition of two atomic ensembles coupled to a lossy cavity [39, 40]. Although the observed features may appear to be remarkably similar, we want to emphasize that the dynamical phase transition discussed here is fundamentally distinct. The emission in the SSR and bistable SSR phases always appear with a monochromatic but possibly bistable frequency. On the other hand, the unsynchronized phase in Refs. [39, 40] shows a beating of two frequencies that results from simultaneous output. Moreover, the synchronization transition in Refs. [39, 40] appears if the collective linewidth becomes comparable to the frequency splitting of the two ensembles. Here, however, the transition between SSR and bistable SSR appears if the atoms travel exactly half a wavelength during the transit time  $\tau$ , i.e.  $k_c v_z \tau = \pi$ , independent of  $NT_c$ . Therefore the transition from SSR to bistable SSR results from the dipole accumulating a phase when it travels through the cavity mode function.

While this Letter is dedicated to a fundamental study of the SSR to bistable SSR transition, we expect that the simplicity and the sensitivity of this system close to the transition point might be useful for developing practical devices such as sensors. From a broader perspective,

although there is a great variety of works that study collective behavior of trapped atomic ensembles, this work might be one of the first stepping stones towards the investigation of collective effects in atomic beams traversing optical cavities. Such systems could make certain practical applications feasible due to the absence of external trapping and because common state preparation steps such as optical pumping and cooling can be performed outside of the cavity [51].

This work was supported by the NSF PFC Grant No. PHY 1734006 and the DARPA and ARO Grant No. W911NF-16-1-0576.

---

[1] D. Nagy, G. Szirmai, and P. Domokos, *Eur. Phys. J. D* **48**, 127 (2008).

[2] J. Larson, B. Damski, G. Morigi, and M. Lewenstein, *Phys. Rev. Lett.* **100**, 050401 (2008); J. Larson, S. Fernández-Vidal, G. Morigi, and M. Lewenstein, *New J. Phys.* **10**, 045002 (2008).

[3] K. Baumann, C. Guerlin, F. Brennecke, and T. Esslinger, *Nature (London)* **464**, 1301 (2010).

[4] J. Léonard, A. Morales, P. Zupancic, T. Esslinger, and T. Donner, *Nature (London)* **543**, 87 (2017).

[5] J. Léonard, A. Morales, P. Zupancic, T. Donner, and T. Esslinger, *Science* **358**, 1415 (2017).

[6] H. Habibian, A. Winter, S. Paganelli, H. Rieger, and G. Morigi, *Phys. Rev. Lett.* **110**, 075304 (2013).

[7] R. Landig, L. Hruba, N. Dogra, M. Landini, R. Mottl, T. Donner, and T. Esslinger, *Nature (London)* **532**, 476 (2016).

[8] R. M. Kroese, Y. Guo, V. D. Vaidya, J. Keeling, and B. L. Lev, *Phys. Rev. Lett.* **121**, 163601 (2018).

[9] M. Landini, N. Dogra, K. Kroeger, L. Hruba, T. Donner, and T. Esslinger, *Phys. Rev. Lett.* **120**, 223602 (2018).

[10] N. Dogra, M. Landini, K. Kroeger, L. Hruba, T. Donner, and T. Esslinger, *Science* **366**, 1496 (2019).

[11] P. Domokos and H. Ritsch, *Phys. Rev. Lett.* **89**, 253003 (2002).

[12] A. T. Black, H. W. Chan, and V. Vuletić, *Phys. Rev. Lett.* **91**, 203001 (2003).

[13] H. Ritsch, P. Domokos, F. Brennecke, and T. Esslinger, *Rev. Mod. Phys.* **85**, 553 (2013).

[14] S. Schütz and G. Morigi, *Phys. Rev. Lett.* **113**, 203002 (2014).

[15] S. Schütz, S. B. Jäger, and G. Morigi, *Phys. Rev. Lett.* **117**, 083001 (2016).

[16] T. Keller, V. Torggler, S. B. Jäger, S. Schütz, H. Ritsch, and G. Morigi, *New J. Phys.* **20**, 025004 (2018).

[17] M. H. Schleier-Smith, I. D. Leroux, and V. Vuletic, *Phys. Rev. Lett.* **104**, 073604 (2010).

[18] L. Pezzè, A. Smerzi, M. K. Oberthaler, R. Schmied, and P. Treutlein, *Rev. Mod. Phys.* **90**, 035005 (2018).

[19] R. J. Lewis-Swan, M. A. Norcia, J. R. K. Cline, J. K. Thompson, and A. M. Rey, *Phys. Rev. Lett.* **121**, 070403 (2018).

[20] A. Shankar, G. P. Greve, B. Wu, J. K. Thompson, and M. J. Holland, *Phys. Rev. Lett.* **122**, 233602 (2019).

[21] A. Shankar, L. Salvi, M. L. Chiofalo, N. Poli, and M. J. Holland, *Quantum Sci. Technol.* **4**, 045010 (2019).

[22] D. Meiser, J. Ye, D. R. Carlson, and M. J. Holland, *Phys. Rev. Lett.* **102**, 163601 (2009).

[23] J. G. Bohnet, Z. Chen, J. M. Weiner, D. Meiser, M. J. Holland, and J. K. Thompson, *Nature (London)* **484**, 78 (2012).

[24] M. Gross, S. Haroche, *Phys. Rep.* **93**, 301 (1982).

[25] R. H. Dicke, *Phys. Rev.* **93**, 99 (1954).

[26] D. Meiser and M. J. Holland, *Phys. Rev. A* **81**, 033847 (2010).

[27] D. Meiser and M. J. Holland, *Phys. Rev. A* **81**, 063827 (2010).

[28] J. G. Bohnet, Z. Chen, J. M. Weiner, K. C. Cox, and J. K. Thompson, *Phys. Rev. A* **89**, 013806 (2014).

[29] M. A. Norcia and J. K. Thompson, *Phys. Rev. X* **6**, 011025 (2016).

[30] M. A. Norcia, M. N. Winchester, J. R. K. Cline, and J. K. Thompson, *Sci. Adv.* **2**, e1601231 (2016).

[31] K. Tucker, B. Zhu, R. J. Lewis-Swan, J. Marino, F. Jimenez, J. G. Restrepo, and A. M. Rey, *New J. Phys.* **20**, 123033 (2018).

[32] F. Iemini, A. Russomanno, J. Keeling, M. Schirò, M. Dalmonte, and R. Fazio, *Phys. Rev. Lett.* **121**, 035301 (2018).

[33] Z. Gong, R. Hamazaki, and M. Ueda, *Phys. Rev. Lett.* **120**, 040404 (2018).

[34] H. Keßler, J. G. Cosme, M. Hemmerling, L. Mathey, and A. Hemmerich, *Phys. Rev. A* **99**, 053605 (2019).

[35] B. Zhu, J. Marino, N. Y. Yao, M. D. Lukin, and E. A. Demler, *New J. Phys.* **21**, 073028 (2019).

[36] H. Mori and Y. Kuramoto, *Dissipative Structures and Chaos* (Springer, Berlin, 1998).

[37] J. A. Acebrón, L. L. Bonilla, C. J. Pérez Vicente, F. Ritort, and R. Spigler, *Rev. Mod. Phys.* **77**, 137 (2005).

[38] B. Zhu, J. Schachenmayer, M. Xu, F. Herrera, J. G. Restrepo, M. J. Holland, and A. M. Rey, *New J. Phys.* **17**, 083063 (2015).

[39] M. Xu, D. A. Tieri, E. C. Fine, J. K. Thompson, and M. J. Holland, *Phys. Rev. Lett.* **113**, 154101 (2014).

[40] J. M. Weiner, K. C. Cox, J. G. Bohnet, and J. K. Thompson, *Phys. Rev. A* **95**, 033808 (2017).

[41] D. Barberena, R. J. Lewis-Swan, J. K. Thompson, and A. M. Rey, *Phys. Rev. A* **99**, 053411 (2019).

[42] M. A. Norcia, R. J. Lewis-Swan, J. R. K. Cline, B. Zhu, A. M. Rey, and J. K. Thompson, *Science* **361**, 259 (2018).

[43] J. A. Muniz, D. Barberena, R. J. Lewis-Swan, D. J. Young, J. R. K. Cline, A. M. Rey, and J. K. Thompson, *Nature* **580**, 602 (2020).

[44] S. B. Jäger, J. Cooper, M. J. Holland, and G. Morigi, *Phys. Rev. Lett.* **123**, 053601 (2019).

[45] S. B. Jäger, M. J. Holland, and G. Morigi, *Phys. Rev. A* **101**, 023616 (2020).

[46] A. Campa, T. Dauxois, and S. Ruffo, *Phys. Rep.* **480**, 57 (2009).

[47] J. Schachenmayer, A. Pikovski, and A. M. Rey, *Phys. Rev. X* **5**, 011022 (2015).

[48] See Supplemental Material.

[49] E. Abraham and S. D. Smith, *Rep. Prog. Phys.* **45**, 815 (1982).

[50] S. Sachdev, *Quantum Phase Transitions*, 2nd ed. (Cambridge University, Cambridge, England, 2011).

[51] C.-C. Chen, S. Bennetts, R. G. Escudero, B. Pasquiou, and F. Schreck, *Phys. Rev. Applied* **12**, 044014 (2019).

## Supplemental Material: Steady-state and bistable superradiant phases of an atomic beam traversing an optical cavity

### Mean-field description of the dynamics

In this section we present a mean-field analysis of Eqs. (1-3) of the main article. Exchanging the noisy variables  $s_a$  with  $a \in \{x, y, z\}$  and  $J_a$  by their expectation values we obtain the mean-field equations

$$\frac{\partial \langle s_x \rangle}{\partial t} + \mathbf{v} \cdot \nabla_{\mathbf{x}} \langle s_x \rangle = \frac{\Gamma_c}{2} \eta(\mathbf{x}) \langle J_x \rangle \langle s_z \rangle, \quad (\text{S1})$$

$$\frac{\partial \langle s_y \rangle}{\partial t} + \mathbf{v} \cdot \nabla_{\mathbf{x}} \langle s_y \rangle = \frac{\Gamma_c}{2} \eta(\mathbf{x}) \langle J_y \rangle \langle s_z \rangle, \quad (\text{S2})$$

$$\frac{\partial \langle s_z \rangle}{\partial t} + \mathbf{v} \cdot \nabla_{\mathbf{x}} \langle s_z \rangle = -\frac{\Gamma_c}{2} \eta(\mathbf{x}) [\langle J_x \rangle \langle s_x \rangle + \langle J_y \rangle \langle s_y \rangle]. \quad (\text{S3})$$

These equations together with the spatially homogeneous boundary conditions  $\langle s_z(x = -w, z) \rangle = N/(2w\lambda)$  and  $\langle s_x(x = -w, z) \rangle = 0 = \langle s_y(x = -w, z) \rangle$  form the mean-field version of the stochastic equations presented in the main text. Here,  $N$  is the number of atoms in the cavity,  $w$  is the cavity waist and  $\lambda = 2\pi/k_c$  is the wavelength of the light.

### Non-superradiant phase

Without any noise, the system will always remain in a non-superradiant configuration  $\langle s_x \rangle = 0 = \langle s_y \rangle$ , and consequently  $\langle J_x \rangle = 0 = \langle J_y \rangle$ . In this case the particles remain in the excited state

$$\langle s_z \rangle = \frac{N}{2w\lambda}. \quad (\text{S4})$$

However, noise will give rise to fluctuations around this mean-field solution and the system will eventually undergo emission if these fluctuations are unstable.

This behavior can be understood by deriving differential equations for the fluctuations  $\delta s_a = s_a - \langle s_a \rangle$  ( $a \in \{x, y\}$ ) that read

$$\frac{\partial \delta s_a}{\partial t} + \mathbf{v} \cdot \nabla_{\mathbf{x}} \delta s_a = \frac{N\Gamma_c}{4w\lambda} \eta(\mathbf{x}) \delta J_a. \quad (\text{S5})$$

In order to derive this differential equation we neglected second order terms in the fluctuations. Using the Laplace transformation,  $L[f](\nu) = \int_0^\infty e^{-\nu t} f(t) dt$ , we can rewrite this in the form

$$L[\delta J_a] = \frac{\int d\mathbf{x} \int_0^\infty dt e^{-\nu t} \eta(\mathbf{x} + \mathbf{v}t) \delta s_a(\mathbf{x}, 0)}{1 - \frac{N\Gamma_c}{4w\lambda} \int d\mathbf{x} \int_0^\infty dt e^{-\nu t} \eta(\mathbf{x} + \mathbf{v}t) \eta(\mathbf{x})}, \quad (\text{S6})$$

where  $\delta s_a(\mathbf{x}, 0)$  is an initial condition and we have used the notation  $\int d\mathbf{x} f(\mathbf{x}) = \int_{-w}^w dx \int_0^\lambda dz f(x, z)$  for any function  $f(\mathbf{x}) = f(x, z)$ . Back-transformation into

the time domain leads to the solution of  $\delta J_a$ . We are interested in the stability of this solution, that is, whether  $\delta J_a$  is exponentially damped or exponentially grows. This behavior can be studied using the dispersion relation, that is the denominator of Eq. (S6), whose roots determine the exponents in the time domain. The dispersion relation reads

$$D(\nu) = 1 - \frac{N\Gamma_c}{4w\lambda} \int d\mathbf{x} \int_0^\infty dt e^{-\nu t} \eta(\mathbf{x} + \mathbf{v}t) \eta(\mathbf{x}). \quad (\text{S7})$$

The long-time behavior of  $\delta J_a \propto e^{\nu_0 t}$  is determined by the root  $\nu_0$  of  $D(\nu)$  with the largest real part. If  $\nu_0$  has a negative real part the non-superradiant state is stable and  $\nu_0$  determines the rate of decay of fluctuations. On the other hand, if  $\nu_0$  has a positive real part the fluctuations will exponentially grow and thereby seed a superradiant emission from the ensemble.

In the main text we use the mode function

$$\eta(\mathbf{x}) = [\Theta(x + w) - \Theta(x - w)] \cos(k_c z) \quad (\text{S8})$$

to calculate the critical condition  $\text{Re}(\nu_0) = 0$  that is visible in Fig. 1c as a solid line.

### Superradiant phases

This section is dedicated to the mean-field description of the superradiant phase. As we report in the main text, there are two different superradiant phases. Both can be classified by a non-vanishing collective dipole with a constant length. However, in one phase the collective dipole oscillates with a non-vanishing frequency  $\omega$  (bistable SSR) while in the other regime the phase of the collective dipole remains almost constant (SSR).

In order to analyze this behavior we use the mean-field equations

$$\frac{\partial \langle s \rangle}{\partial t} + \mathbf{v} \cdot \nabla_{\mathbf{x}} \langle s \rangle = \frac{\Gamma_c}{2} \eta(\mathbf{x}) \langle s_z \rangle \langle J \rangle, \quad (\text{S9})$$

$$\frac{\partial \langle s_z \rangle}{\partial t} + \mathbf{v} \cdot \nabla_{\mathbf{x}} \langle s_z \rangle = -\Gamma_c \eta(\mathbf{x}) [\langle J^* \rangle \langle s \rangle + \langle s^* \rangle \langle J \rangle], \quad (\text{S10})$$

that are now presented for the complex dipole  $s = (s_x - is_y)/2$  and  $J = \int d\mathbf{x} s$ , and  $(\cdot)^*$  denotes complex conjugation.

We use the parametrization

$$\langle s \rangle = \frac{N}{4w\lambda} e^{-i\phi(\mathbf{x}, t)} \sin(K(\mathbf{x}, t)), \quad (\text{S11})$$

$$\langle s_z \rangle = \frac{N}{2w\lambda} \cos(K(\mathbf{x}, t)), \quad (\text{S12})$$

with space and time dependent angles  $\phi(\mathbf{x}, t)$  and  $K(\mathbf{x}, t)$ .

In both superradiant phases, SSR and bistable SSR, we expect a behavior for  $\phi(\mathbf{x}, t)$  according to

$$\phi(\mathbf{x}, t) = \omega t + \psi(\mathbf{x}), \quad (\text{S13})$$

where  $\omega$  is the frequency of the emitted light and  $\psi$  is a position dependent but time independent phase. Subsequently, assuming  $K$  is not explicitly time dependent, we obtain the following coupled differential equations for  $\psi$  and  $K$

$$\omega + \mathbf{v} \cdot \nabla_{\mathbf{x}} \psi = -\Gamma_c \eta(\mathbf{x}) |\langle J \rangle| \sin(\psi) \cot(K), \quad (\text{S14})$$

$$\mathbf{v} \cdot \nabla_{\mathbf{x}} K = \Gamma_c \eta(\mathbf{x}) |\langle J \rangle| \cos(\psi). \quad (\text{S15})$$

These equations can be solved together with the two equations emerging from the real and imaginary parts of  $\int d\mathbf{x} \langle s \rangle e^{i\omega t} = |\langle J \rangle|$ . We have derived these equations, without loss of generality, under the assumption that  $\langle J \rangle$  points in  $x$  direction at  $t = 0$ . The solutions of this nonlinear system lead to the results that are shown as solid blue and red lines in Fig. 3a-d.

### Phase diffusion and the linewidth in the SSR phase

In this section we describe our calculation of the phase diffusion in the SSR phase. In order to derive the phase diffusion we need to include noise processes in our analysis. We can represent Eqs. (1-3) in the main text with respect to an arbitrary rotation in the  $x$ - $y$  plane of the dipole. Assuming the system has a collective dipole with some arbitrary phase  $\varphi$  we can rotate into a frame such that  $J_{\parallel} \sim N$  and  $J_{\perp} \sim \sqrt{N}$ . The direction corresponding to  $J_{\parallel}$  is the direction of the collective dipole while the vertical direction  $J_{\perp}$  is solely dominated by fluctuations. The dynamics of the vertical direction is given by

$$\frac{\partial s_{\perp}}{\partial t} + \mathbf{v} \cdot \nabla_{\mathbf{x}} s_{\perp} \approx \frac{\Gamma_c}{2} \eta(\mathbf{x}) J_{\perp} s_{z,\text{st}} + \mathcal{S}_{\perp}, \quad (\text{S16})$$

where we have dropped second order terms in the fluctuations and are therefore able to substitute the mean-field solution for  $s_z$  given by

$$s_{z,\text{st}} = \frac{N}{2w\lambda} \cos(K(\mathbf{x})), \quad (\text{S17})$$

where  $K$  is the solution of Eq. (S15) for  $\omega = 0 = \psi$ . Equation (S16) includes cavity noise described by the quantity  $\mathcal{S}_{\perp}(\mathbf{x}, t) = \eta(\mathbf{x}) \mathcal{F}_{\perp} s_z$  with  $\langle \mathcal{F}_{\perp}(t) \rangle = 0$  and  $\langle \mathcal{F}_{\perp}(t) \mathcal{F}_{\perp}(t') \rangle = \Gamma_c \delta(t - t')$ . Beside the cavity noise it also includes the noisy boundary condition that arises from the introduction of new atoms  $s_{\perp}(x = -w, z, t) = W_{\perp}(z, t)$ , with  $\langle W_{\perp}(z, t) \rangle = 0$  and  $\langle W_{\perp}(z, t) W_{\perp}(z', t') \rangle = N/(2w\lambda) \delta(z - z') \delta(t - t')/v_x$ .

Using the Laplace transformation we can derive

$$L[J_{\perp}] \approx \frac{L[J_{W_{\perp}}] + 2 \frac{1 - D_{\perp}(\nu)}{\Gamma_c} L[\mathcal{S}_{\perp}]}{D_{\perp}(\nu)}, \quad (\text{S18})$$

where

$$J_{W_{\perp}}(t) = \int d\mathbf{x} \eta(\mathbf{x} + \mathbf{v}t) W_{\perp} \left( z - \frac{v_z x}{v_x}, p_z, -\frac{x}{v_x} \right), \quad (\text{S19})$$

arises from the initial projection noise and

$$D_{\perp}(\nu) = \nu \frac{\int_0^{\infty} e^{-\nu t} dt \int d\mathbf{x} \eta(\mathbf{x} + \mathbf{v}t) s_{\parallel,\text{st}}(\mathbf{x})}{J_{\parallel,\text{st}}}, \quad (\text{S20})$$

is the dispersion relation of the Goldstone mode of the collective dipole. Here, we have used

$$s_{\parallel,\text{st}} = \frac{N}{2w\lambda} \sin(K(\mathbf{x})), \quad (\text{S21})$$

and  $J_{\parallel,\text{st}} = \int d\mathbf{x} \eta(\mathbf{x}) s_{\parallel,\text{st}}$ . Assuming that  $\nu = 0$  is the largest zero of  $D_{\perp}(\nu)$  we can assume that for long times

$$J_{\perp} \approx \frac{\int_0^t dt' [A_1(t') + A_2(t')]}{C_0}, \quad (\text{S22})$$

with

$$A_1(t') = \int d\mathbf{x} \eta(\mathbf{x} + \mathbf{v}t') W_{\perp} \left( z - \frac{v_z x}{v_x}, -\frac{x}{v_x} \right), \quad (\text{S23})$$

$$A_2(t') = \frac{2\mathcal{S}_{\perp}(t')}{\Gamma_c}, \quad (\text{S24})$$

and where the denominator is given by

$$C_0 = \lim_{\nu \rightarrow 0} \frac{D_{\perp}(\nu)}{\nu} = \frac{\int_0^{\infty} dt \int d\mathbf{x} \eta(\mathbf{x} + \mathbf{v}t) s_{\parallel,\text{st}}(\mathbf{x})}{J_{\parallel,\text{st}}}. \quad (\text{S25})$$

Equation (S22) describes a diffusive dynamics vertical to the direction of the collective dipole with length  $J_{\parallel,\text{st}}$ . Using  $d\varphi/(dt) \approx J_{\parallel,\text{st}}^{-1} dJ_{\perp}/(dt)$ , we find that

$$\Delta\varphi(t) = \varphi(t) - \varphi(0) \approx \frac{\int_0^t dt' [A_1(t') + A_2(t')]}{C_0 J_{\parallel,\text{st}}}. \quad (\text{S26})$$

The linewidth can now be calculated from the fluctuations of the phase

$$\Gamma = \lim_{t \rightarrow \infty} \frac{\langle \Delta\varphi(t)^2 \rangle}{t}. \quad (\text{S27})$$

The result of this calculation is plotted in Fig. 3e-f as solid blue and red lines in the SSR phase.

This calculation can also be used to determine the phase boundaries between SSR and bistable SSR. At the transition the linewidth diverges that is visible here because of  $C_0 = 0$ . For  $k_c v_z \tau = \pi$  the integral over  $t$  and  $z$  in Eq. (S25) vanishes. This determines the threshold (dashed line) in Fig. 1c between the SSR and bistable SSR phases and the gray vertical dashed lines in Fig. 3.

## Mode hopping probability

This section provides additional information about the jumps between the two bistable solutions in the bistable SSR phase (see Fig. 2b in the main text). To analyze this effect we have defined the phase difference

$$\Delta\varphi(t) = \arg \left( \int_{t_0}^{t_1} dt'_0 \frac{\langle J^*(t+t'_0)J(t'_0) \rangle}{t_1 - t_0} \right), \quad (\text{S28})$$

where  $\arg(\cdot)$  denotes the complex argument and  $t_0$  and  $t_1$  are initial time and final time of a time average. In Fig. S1a we have plotted the phase  $\Delta\varphi(t)$  as function of the time  $t$  in units of  $\tau$  and for different trajectories in different color codings. The parameters are the same as in Fig. 2b of the main text, i.e.,  $k_c v_z \tau = 2\pi \times 0.8$  and  $N\Gamma_c \tau = 30$ . We observe a linear dependence of

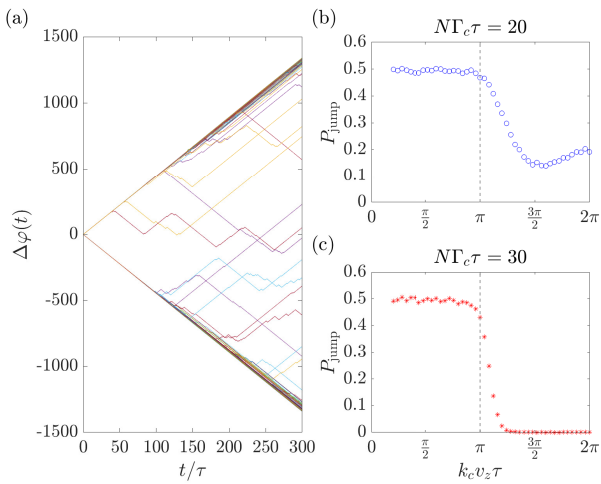


FIG. S1. (a) The phase difference  $\Delta\varphi(t)$  (Eq. (S28)) as a function of time in units of  $\tau$  for  $t_0 = 10\tau$  and  $t_1 = 1700\tau$  and total simulation time  $t_{\text{sim}} = 2000\tau$  for  $N = 800$ . Subplot (b) and (c) show the jump probability  $P_{\text{jump}}$  (Eq. (S30)) for different values of  $k_c v_z \tau$  for  $N\Gamma_c \tau = 20$  and  $N\Gamma_c \tau = 30$ , respectively. For the simulations we used  $t_{\text{sim}} = 100\tau$  and  $N = 800$  and started the analysis after  $t_0 = 10\tau$  where the system reached for good approximation the stationary state. The value of  $\Delta\varphi(t)$  for each trajectory is calculated according to Eq. (S28) without the time average for  $t_1 \rightarrow t_0$ . With the notations prior to Eq. (S30) we have used  $t_{\text{max}} = 90\tau$  that we split into  $M = 20$  bins. The gray dashed vertical line shows the threshold between SSR and bistable SSR phase.

the phase with two slopes that are either negative or positive. These slopes correspond to a negative frequency  $\omega\tau \approx -4.46$  and positive frequency  $\omega\tau \approx 4.46$  (compare Fig. 2b in the main text). While most of the trajectories preserve their initial slope, there are a few trajectories

that hop between the slopes corresponding to the positive and negative frequencies.

In order to analyze this effect we calculate the probability for the occurrence of a jump from the negative to the positive frequency. For this we divide the time interval  $[0, t_{\text{max}}]$  of every trajectory  $\Delta\varphi(t)$  into  $M$  equal distant time bins  $[(m-1)\Delta t, m\Delta t]$  with  $m = 1, \dots, M$  and  $\Delta t = t_{\text{max}}/M$ . Within this time bin we calculate an average frequency

$$\omega(m) = \frac{1}{\Delta t} \int_{(m-1)\Delta t}^{m\Delta t} dt' \frac{d\Delta\varphi(t')}{dt'}. \quad (\text{S29})$$

Using the average frequency we now decide if a frequency jump appears if  $\omega(m)\omega(m+1) < 0$  for  $m = 1, \dots, M-1$ . Counting now the number of jumps of all trajectories,  $N_{\text{jump}}$ , and dividing by the maximum number of jumps possible  $N_{\text{total}} = (M-1) \times \mathcal{T}$ , where  $\mathcal{T}$  is the number of trajectories, we get

$$P_{\text{jump}} = \frac{N_{\text{jump}}}{N_{\text{total}}} \quad (\text{S30})$$

for the jump probability. We want to mention that this definition depends on the length of the time bins  $\Delta t$ .

The jump probability is shown in Fig. S1b-c for various values of  $k_c v_z \tau$  across the phase transition from SSR to bistable SSR and for  $N\Gamma_c \tau = 20$  and  $N\Gamma_c \tau = 30$ , respectively. The simulations are the same as in Fig. 3 in the main text. We see that  $P_{\text{jump}}$  for both values of  $N\Gamma_c \tau$  well inside of the SSR phase is close to  $P_{\text{jump}} \approx 0.5$ . This can be explained by the fact that  $\Delta\varphi$  diffuses. In this case, after every time bin, the total phase gains with probability 0.5 a positive or negative phase. Beyond the transition point,  $k_c v_z \tau = \pi$ , we observe in both cases a decrease of this jump probability. For  $N\Gamma_c \tau = 30$  (Fig. S1c), we observe that the jump probability drops to a value very close to  $P_{\text{jump}} \approx 0$ . This emphasizes that the switch between a negative and a positive frequency becomes very improbable. While we also see a decrease of the jump probability for  $N\Gamma_c \tau = 20$  (Fig. S1b) after the critical point, a jump is still much more likely than for  $N\Gamma_c \tau = 30$ . Moreover, we observe that the jump probability shows a local minimum very close to the local maximum of the amplitude of the collective dipole (see Fig. 3a in the main text). Therefore we propose that the reason for this effect is the more pronounced contribution of noise with respect to the mean value of the collective dipole. We expect that the jump probability will decrease in the bistable SSR phase for larger particle number  $N$  when the ratio of noise to the mean value of the collective dipole is further reduced.